AGU PUBLICATIONS

Geophysical Research Letters

RESEARCH LETTER

10.1002/2016GL071230

Key Points:

- Scattering component of airborne radio-echo sounding surface echo is mapped across Devon Ice Cap
- The scattering signal component is mainly affected by the near-surface firn stratigraphy
- Effects from surface roughness on the scattering component are minor

Correspondence to:
A. Rutishauser,
rutishau@ualberta.ca

Citation:
Rutishauser, A., C. Grima, M. Sharp, D. D. Blankenship, D. A. Young, F. Cawkwell, and J. A. Dowdeswell (2016), Characterizing near-surface firn using the scattered signal component of the glacier surface return from airborne radio-echo sounding, *Geophys. Res. Lett.*, *43*, 12,502–12,510, doi:10.1002/2016GL071230.

Received 15 SEP 2016
Accepted 30 NOV 2016
Accepted article online 5 DEC 2016
Published online 30 DEC 2016

Characterizing near-surface firn using the scattered signal component of the glacier surface return from airborne radio-echo sounding

Anja Rutishauser[1], Cyril Grima[2], Martin Sharp[1], Donald D. Blankenship[2], Duncan A. Young[2], Fiona Cawkwell[3], and Julian A. Dowdeswell[4]

[1]Department of Earth and Atmospheric Sciences, University of Alberta, Edmonton, Alberta, Canada, [2]Institute for Geophysics, University of Texas at Austin, Austin, Texas, USA, [3]Department of Geography, University College Cork, Cork, Ireland, [4]Scott Polar Research Institute, University of Cambridge, Cambridge, UK

Abstract We derive the scattered component (hereafter referred to as the incoherent component) of glacier surface echoes from airborne radio-echo sounding measurements over Devon Ice Cap, Arctic Canada, and compare the scattering distribution to firn stratigraphy observations from ground-based radar data. Low scattering correlates to laterally homogeneous firn above 1800 m elevation containing thin, flat, and continuous ice layers and below 1200 m elevation where firn predominantly consists of ice. Increased scattering between elevations of 1200–1800 m corresponds to firn with inhomogeneous, undulating ice layers. No correlation was found to surface roughness and its theoretical incoherent backscattering values. This indicates that the scattering component is mainly influenced by the near-surface firn stratigraphy, whereas surface roughness effects are minor. Our results suggest that analyzing the scattered signal component of glacier surface echoes is a promising approach to characterize the spatial heterogeneity of firn that is affected by melting and refreezing processes.

1. Introduction

Glaciers and ice caps in the Canadian Arctic Archipelago (CAA) contain the largest mass of ice outside Greenland and Antarctica [*Radić and Hock*, 2011] and are projected to be significant contributors to sea level rise over the next century [*Radić and Hock*, 2011; *Radić et al*., 2013; *Vaughan et al*., 2013; *Harig and Simons*, 2016]. With recent summer warming, surface melt on these ice masses has intensified and extended to higher elevations [*Fisher et al*., 2011; *Sharp et al*., 2011; *Bezeau et al*., 2013; *Gascon et al*., 2013; *Mortimer et al*., 2016]. In the accumulation area, where firn temperatures are below freezing, meltwater percolates into the firn and refreezes as ice layers. Repeat firn cores, borehole temperature profiles, and ground-penetrating radar surveys document major changes in the firn stratigraphy of CAA ice caps and glaciers over the past 10–15 years [*Bezeau et al*., 2013; *Gascon et al*., 2013], but spatially extensive measurements are sparse.

Knowledge of the near-surface firn stratigraphy is important for interpreting altimetrically derived measurements of glacier surface height in terms of changes in glacier mass balance [*Parry et al*., 2007]. The glacier surface height in the accumulation area is affected by changes in the near-surface firn density, even in the absence of mass changes [*Braithwaite et al*., 1994]. Ice layer formation by meltwater percolation/refreezing can significantly increase firn densification rates, causing a lowering of the glacier surface height. Strong density contrasts associated with ice layers in the firn can generate ambiguous reflections in satellite radar altimetry data, leading to a difference between the measured elevation and that of the actual glacier surface [*Gray et al*., 2015].

Recent studies used properties of the glacier surface reflection from airborne radio-echo sounding (RES) measurements to determine the near-surface firn density and the surface roughness of Thwaites Glacier, West Antarctica [*Grima et al*., 2014a, 2014b; *Schroeder et al*., 2016]. However, direct density estimates from the RES surface signal are only feasible if the firn density increases continuously with depth (i.e., steady state accumulation) [*Grima et al*., 2014b], which is not the case for CAA ice caps where there are often ice layers in the firn. Here we investigate the use of the scattering signal component of the RES glacier surface reflection to characterize near-surface firn stratigraphies affected by melting and refreezing processes. We apply the Radar Statistical Reconnaissance (RSR) method [*Grima et al*., 2014a] to airborne RES measurements from Devon Ice Cap (DIC) to calculate the scattering signal component. We compare this component to the

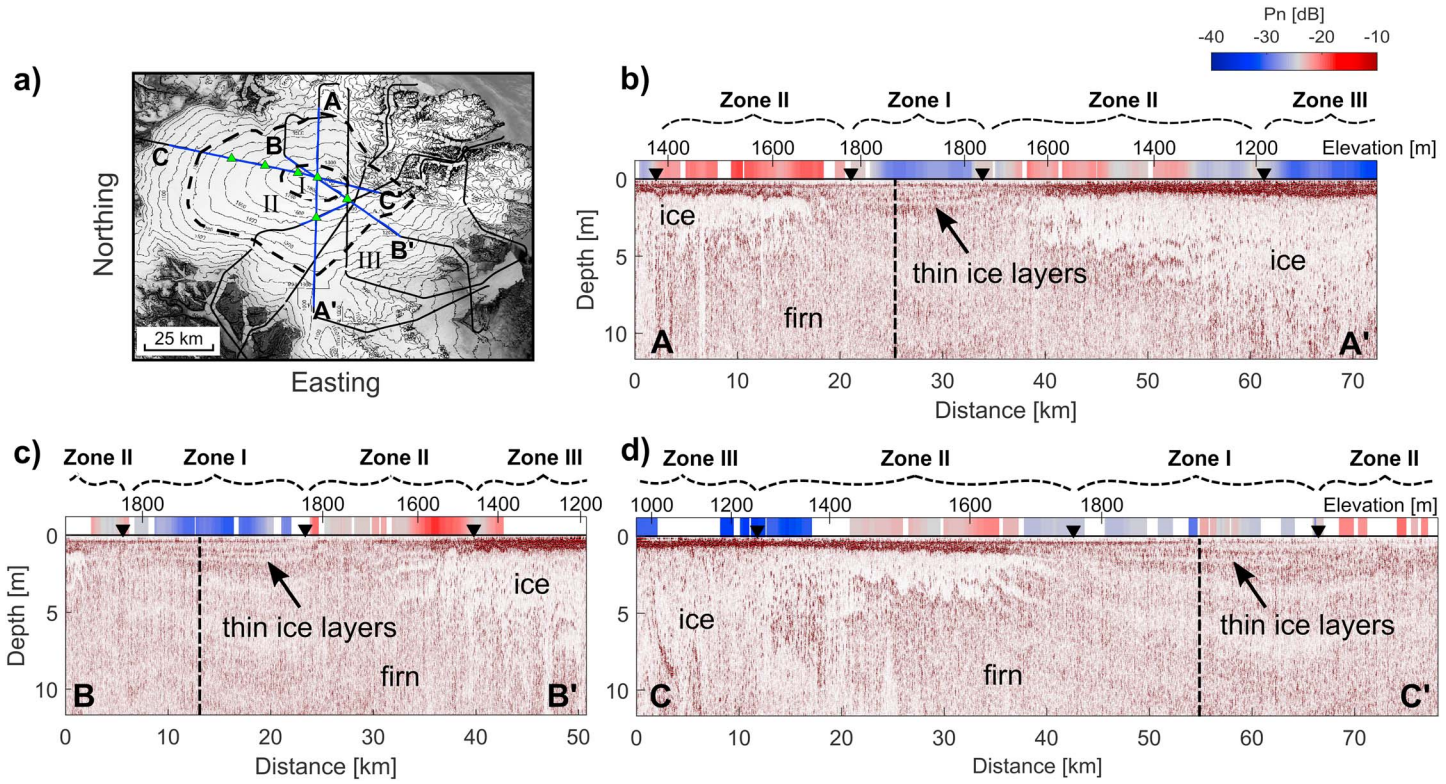

Figure 1. (a) Map of the airborne (black) and ground-based RES profiles (blue) over Devon Ice Cap, along with the location of the shallow firn cores (green). Black dashed lines indicate the firn facies zone boundaries. (b–d) Ground-based RES profiles revealing the firn stratigraphy. Dashed lines mark the location where the three profiles cross (~1880 m elevation), and the black markers indicate the locations of the picked firn zone boundaries. The scattered component of the airborne RES surface echo (P_n) is plotted in color code above each profile.

near-surface firn stratigraphy revealed by ground-based RES measurements and to glacier surface roughness estimates and their theoretical backscattering values. We then discuss the relative influences of the near-surface firn stratigraphy and the surface roughness on the scattering component and show that the firn stratigraphy is the predominant influence on signal scattering. This is the first application of the RSR method to an ice cap with a firn layer affected by spatiotemporally complex patterns of melting and refreezing. We argue that the RSR method and analysis of the scattered signal component have potential to characterize such firn stratigraphy.

2. Data and Methods

2.1. Radio-Echo Sounding Data

Airborne RES data were collected over DIC in spring 2014 (Figure 1a) using the University of Texas Institute for Geophysics' High-Capability Radar Sounder (HiCARS) [*Peters et al.*, 2005]. HiCARS transmits chirped pulses at 60 MHz center frequency (i.e., 5 m wavelength) over a 15 MHz bandwidth [*Peters et al.*, 2005]. HiCARS was mounted on board a Basler DC-3 aircraft operated by Kenn Borek Air, and positioning was obtained with a Global Positioning System (GPS) providing a 15 cm root-mean-square (RMS) vertical accuracy and smaller horizontal errors. The resulting radar data set was sampled every ~1 m along the survey transects. The pulse-limited footprint (area illuminated by the radar) at the surface has a diameter of ~235 m for typical aircraft heights above ice (~700 m).

Several of the airborne RES transects were surveyed with a ground-based RES system in spring 2015 (Figure 1a). A PulseEKKO Noggin radar (Sensors & Software Inc.) with antennae operating at 500 MHz center frequency (i.e., 0.6 m wavelength) was mounted on a plastic sled towed by snowmobile, generating a data set sampled every ~0.4 m along track. Positioning was obtained with a Leica Geosystems GPS system providing a 25 cm RMS accuracy. Processing steps for these RES data included dewow filtering, time-zero shift, background

removal, Butterworth band-pass filtering, and the application of a gain function [e.g., *Cassidy*, 2009]. The firn stratigraphy was further documented using six ~11 m long firn cores drilled along the survey transects (Figure 1a) in May 2015. The stratigraphic data were used to validate and interpret the ground-based RES measurements and to determine bulk firn permittivities and the radar wave velocity in firn.

2.2. Determination of the Scattered Signal Component

In airborne RES measurements, a strong signal from the glacier surface (surface echo) is generated by the large contrast in dielectric properties between the atmosphere and snow, firn, or ice. The surface echo is affected by the material properties of the near-surface (e.g., the vertical dielectric profile and homogeneity) with the probed depth being a function of the pulse width (uppermost 5–10 m for the HiCARS signal). The surface echo strength (P) can be expressed as a combination of reflected (specular, deterministic phase interference, P_c) and scattered (random phase interference, P_n) signal components, so that $P = P_c + P_n$ [e.g., *Ulaby et al*., 1986]. P_c is mainly sensitive to the permittivity of the probed subsurface, whereas P_n is dominantly affected by the surface roughness and by inhomogeneous geometries in the subsurface [*Grima et al*., 2014a]. We apply the RSR method to estimate P_c and P_n [*Grima et al*., 2014a, 2014b]. To calculate P_c and P_n, the amplitudes of consecutive surface echoes from a defined along-track baseline (1 km, equivalent to ~1000 echoes, repeated every 50 m) are combined in a statistical distribution. The resulting echo amplitude distributions are then best fitted with an analytically derived stochastic envelope (homodyned *K*-distribution, HK) which is parameterized with the signal components P_c and P_n [*Destrempes and Cloutier*, 2010]. The scattering model assumes statistical stationarity of roughness effects over the sampled space (1 km baseline); however, the HK distribution allows for reflector/scatterer clustering (i.e., nonstationarity) over the radar footprint [*Destrempes and Cloutier*, 2010; *Grima et al*., 2014a].

Although scattering values are only analyzed qualitatively, P_c and P_n values are calibrated by a comparison between the calculated radar reflectance P_c (roughness corrected) and the theoretical radar reflectance generated by an air-glacier ice interface (−11.08 dB) at locations where nadir looking camera pictures taken during the airborne RES survey showed exposures of bare ice. P_n values from areas where the correlation coefficient of the fit is below 95% and where the airplane roll angle was above 2° were considered unreliable and discarded.

2.3. Surface Roughness and Theoretical Scattering Component

Analytical models that describe backscattering from rough surfaces [e.g., *Elfouhaily and Guérin*, 2004] show that the scattering component of the surface echo is a function of the surface roughness. To investigate roughness effects on the surface echoes, we calculated the RMS roughness from laser altimetry data collected simultaneously with the HiCARS measurements and modeled the theoretical scattered signal component for the resulting roughness. The laser altimeter provides a 2 mm range resolution with a footprint of ~1 m [*Young et al*., 2008], and measurements were made every ~24.5 m along track. The RMS height σ_h is defined as

$$\sigma_h = \sqrt{\frac{1}{M}\sum_{i=1}^{M}\left(z(x_i) - \overline{z}\right)^2} \tag{1}$$

where M is the number of surface height measurements, $z(x_i)$ is the height at location x_i, and $\overline{z}$ is the mean of the surface heights. σ_h was calculated over sliding windows with $M = 7$ (baseline of ~171.5 m along track), and the resulting RMS heights are used to model the theoretical scattered signal component of the surface echo, following *Grima et al.* [2012]

$$P_n = 4k^2 r^2 \sigma_h^2 \left(1 - e^{-\left(\frac{Dkl}{2h}\right)^2}\right) \tag{2}$$

where k is the wave number, $r = (1 - \sqrt{\varepsilon})/(1 + \sqrt{\varepsilon})$ is the surface Fresnel coefficient with ε being the dielectric constant of the firn, D is the footprint diameter at the glacier surface, l is the roughness correlation length, and h is the aircraft range to the surface. As the roughness correlation length is unknown, we assume $l > 10$ m [*Grima et al*., 2014a], for which the exponential of (2) becomes $\ll 1$ and P_n values take on their maximum value. This is supported by RSR-derived surface densities at Thwaites Glacier where the same large correlation length assumption was applied, and the results conform well with expected density values [*Grima et al*., 2014b]. We note that the laser and radar baselines for σ_h used in equation (2) are not the same. The laser baseline used to calculate σ_h is ~171.5 m, whereas the horizontal length over which the radar scattering signal is affected by a given surface roughness is not known precisely; however, it has been estimated to

be a few wavelengths (5–50 m) [*Grima et al.*, 2012]. *Grima et al.* [2014a] showed that radar RMS heights derived from P_n are about 33% smaller than the corresponding laser-derived RMS heights for that specific acquisition platform. Hence, using laser-derived σ_h and assuming $l > 10$ m in equation (2) likely results in an overestimation of the modeled P_n values. The corresponding equation for the coherent signal part P_c can be found in *Grima et al*. [2014a, equation 6].

Although the theoretical scattering signal component is mainly sensitive to the surface roughness, P_n is also a function of the firn permittivity. We use the stratigraphy of six firn cores (Figure 1a) to estimate bulk permittivity values for the uppermost 10 m of firn. Sections of the firn cores showing ice layers are assigned a density of 875 kg/m^3 [*Bezeau et al.*, 2013], whereas sections showing firn are assigned the theoretical depth-dependent density value $\rho(z) = \rho_i - (\rho_i - \rho_s)\exp\left(-\frac{z}{z_\rho}\right)$ [*Cuffey and Paterson*, 2010], where $\rho_i = 875$ kg/m^3 and $\rho_s = 320$ kg/m^3 are the densities of glacier ice and the spring snowpack, respectively [*Bezeau et al.*, 2013]. The resulting average densities (ρ) for each core are converted to bulk permittivity values following the empirical relationship $\varepsilon = (1 + 845 \times 10^{-6}\rho[\text{kg m}^{-3}])^2$ [*Kovacs et al.*, 1995]. From this, average firn permittivity values of 2.3 and 2.7 were used to model P_n in firn Zones I and II, respectively (see section 3.1 for specifications of firn zones). P_n values in firn Zone III were modeled with $\varepsilon = 3.0$ (mostly ice in firn).

In addition to the surface roughness derived from laser altimeter data, we analyzed ground-based roughness measurements from a field campaign on DIC in spring 2004. The surface roughness was measured at 13 locations along a 48 km long transect from near the summit of the ice cap toward the margin in a southerly direction (Figure 2b). At each site, the height of a fixed laser level above the surface was measured at 10 cm intervals along 10 m long profiles oriented parallel (north-south direction) and perpendicular (west-east direction) to the transect. σ_h was calculated using equation (1) for each profile, and the overall mean surface roughness was determined for each site.

3. Results

3.1. Firn Facies From Ground-Based RES

Three ground-based radar echograms (Figures 1b–1d) reveal the stratigraphy of the uppermost ~12 m of the firn. The profiles intersect near the ice cap's summit at ~1880 m elevation and run toward the margins in various directions (Figure 1a). A common elevation-dependent trend is observed in the firn stratigraphy: at the highest elevations (>1750 m), near the center of the ice cap, a few relatively flat and continuous reflections are present within the uppermost ~2 m of firn. These reflections correlate to thin ice layers (<0.18 m thick) identified in firn cores and are interpreted as ice layers formed by refreezing of percolated meltwater. As elevation decreases, the ice layers in the firn thicken and become undulatory. Below ~1200 m elevation the low subsurface radar reflectivity indicates firn consisting mainly of ice, whereas internal reflections within the massive ice layers likely result from interfaces with residual bodies of firn. The massive ice layers form by refreezing of meltwater. Such a stratigraphy where firn is buried beneath ice layers formed by refreezing is a plausible outcome of equilibrium line migration to higher elevations [e.g., *Gascon et al*., 2013]. *Gascon et al.* [2013] describe firn stratigraphies observed on DIC and assess their implications for melt water flow.

To relate the RSR-derived scattering values to firn characteristics (section 3.2), we identify three firn facies zones. These are based on variations in the apparent homogeneity of firn in the ground-based RES data. A laterally homogeneous firn layer extending over an RSR baseline (1 km) is expected to generate surface echoes with a weak scattering signal component. In contrast, firn containing internal inhomogeneities (i.e., undulating ice layers) is expected to cause a higher scattering signal component. On this basis, Zone I is defined as the area where firn contains thin, flat, and mostly continuous ice layers. It is found at elevations above 1750 m surrounding the summit of the ice cap. Zone II is found between 1150 and 1895 m elevation, where the ice layers are undulating and significantly thicker than in Zone I. In Zone III, the uppermost 6 m (the theoretical depth to which the surface echo is affected by a dielectric profile composed of ice) of firn consists predominantly of ice and appears more homogeneous than firn in Zone II. To exclude possible influences from ice flow within outlet glaciers (e.g., crevassing), we constrain Zone III to areas where the glacier surface lies above 900 m elevation. The resulting Zone III spans an elevation range of 900–1435 m and likely includes areas that lie within the ablation zone in some years [*Gascon et al*., 2013].

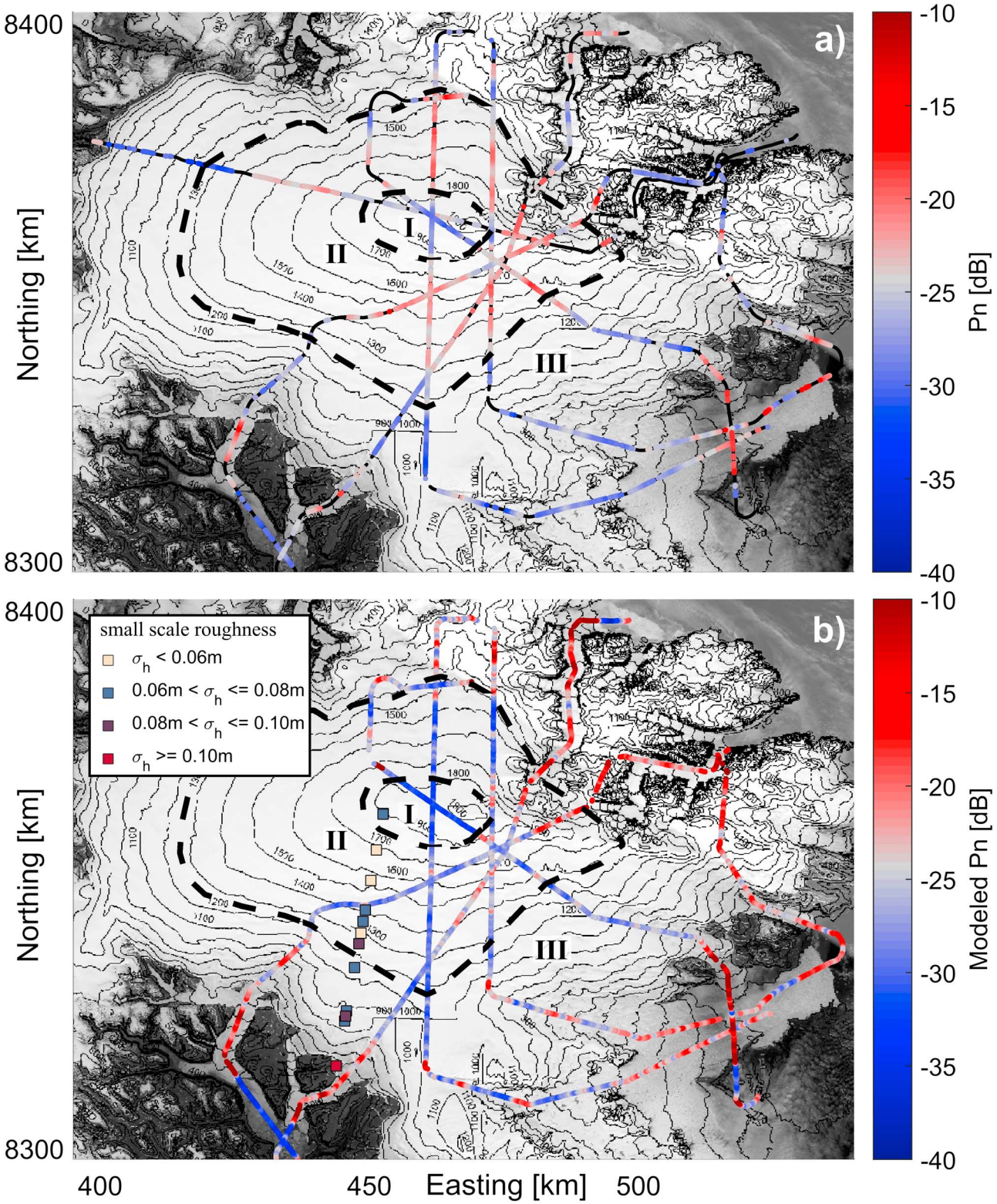

Figure 2. (a) Airborne RES flight tracks over Devon Ice Cap, color coded with the RSR-derived scattered signal component P_n. (b) Laser altimetry transects color coded with the modeled P_n values, indicating the theoretical scattered signal component for the laser-derived surface roughness. To better illustrate large-scale variations, both the RSR-derived and modeled P_n values are smoothed by a moving average filter (2 km along-track window length). The color coded squares indicate small-scale surface roughness values. Black dashed lines indicate the firn facies zone boundaries.

Table 1. Description of the Defined Firn Facies Zones and Results From Statistical Analysis of the Scattering Coefficient Showing the Mean and Standard Deviation of P_n[a]

Firn Facies Zones			Mean P_n (dB)	Standard P_n (dB)	Mean Laser σ_h (m)	Mean Modeled P_n (dB)
Zone I	Thin, continuous ice layers	>1750 m above sea level (asl)	−26.9	2.5	0.05	−31.9
Zone II	Thickening, undulating ice layers	1150–1895 m asl	−23.2	2.8	0.09	−26.9
Zone III	Mostly ice in uppermost 6 m	900–1435 m asl	−27.0	3.4	0.12	−24.5

[a]Additionally, the mean laser-derived RMS height σ_h and modeled scattering coefficient within the three firn zones are listed.

The spatial extent of the firn facies zones is shown in Figure 1a. For airborne RES profiles for which no ground-based RES data were available, the zone boundaries were interpolated using data from neighboring ground-based RES profiles. Since changes in firn characteristics between zones are gradual, we estimate a 5 km along-track error in zone boundary picking.

3.2. Scattering Distribution and Correlation to Firn Facies Zones

The RSR-derived scattering component ranges from −40 to −5 dB across DIC (Figure 2a). Like the firn stratigraphy, P_n values display an elevation-dependent trend forming a circular distribution pattern around the ice cap's center: P_n values are low (<−24 dB) in the summit region, (>1800 m), and below ~1400 m. These two areas are separated by a band of higher P_n values (>−24 dB). Transitions between these high- and low-scattering areas coincide with the defined firn zone transitions (Figure 1) to within 0.4–7 km. The majority lie within the estimated 5 km picking error.

To quantify variations in P_n within the different firn facies zones, we analyzed the P_n values statistically (Table 1). Firn Zones I, II, and III yield mean P_n values of −26.9 dB, −23.2 dB, and −27 dB, respectively. A Kruskal-Wallis test (nonparametric analysis of variance) indicates that P_n values from Zone II are significantly ($p < 0.001$) different from those in Zones I and III, with a 95% confidence level. Thus, the scattering properties of the different firn stratigraphies are statistically significantly different with respect to lateral homogeneity. These results are consistent with the expected pattern of high scattering where near-surface firn is inhomogeneous and low scattering where it is more homogeneous. The high-scattering values in firn Zone II could be explained by the presence of the inhomogeneous, undulating ice layers in the firn, whereas the flat and continuous ice layers in firn Zone I appear to reflect the radar signal coherently. Similarly, the firn stratigraphy in Zone III does not significantly scatter the surface echo, indicating that despite the presence of some residual firn bodies, the probed subsurface appears homogeneous at the frequency and configurations of HiCARS. Higher P_n values near some outlet glacier termini likely result from scattering at crevasses and broken floating ice.

3.3. Effects of Surface Roughness

The good correlation between areas with distinct P_n values and the different firn facies zones suggests that changes in the scattering coefficient are caused by changes in the firn stratigraphy. However, because P_n is also a function of surface roughness, it is important to determine whether there is any relation between P_n and the observed surface roughness. If surface roughness was the major source of signal scattering, a positive correlation would be expected between P_n and roughness [*Grima et al.*, 2014a].

The laser-derived RMS surface roughness of DIC ranges between 0.008 and 5.9 m, with averages for Zones I, II, and III of 0.05 m, 0.09 m, and 0.12 m, respectively (Table 1). The modeled scattered signal components for the observed roughnesses (Figure 2b) are generally lower (−31.9 dB, −26.9 dB, and −24.5 dB for firn Zones I, II, and III, respectively, Table 1) than the RSR-derived scattering values and have a different spatial pattern. This suggests the surface roughness of DIC is not the major influence on the scattered signal component and supports the argument that differences in P_n are due to differences in the near-surface firn stratigraphy. This is reinforced by Figure 3, which shows that the observed P_n values and the laser-derived surface roughnesses are not correlated.

However, given the relatively large point separation of the laser measurements (24.5 m), the laser-derived σ_h values might exclude small, wind-sculpted forms like sastrugi and capture only large-scale surface irregularities. Unfortunately, no smaller scale roughness measurements are available for the period when the data used in this study were collected. Nevertheless, we analyzed ground-based roughness measurements from

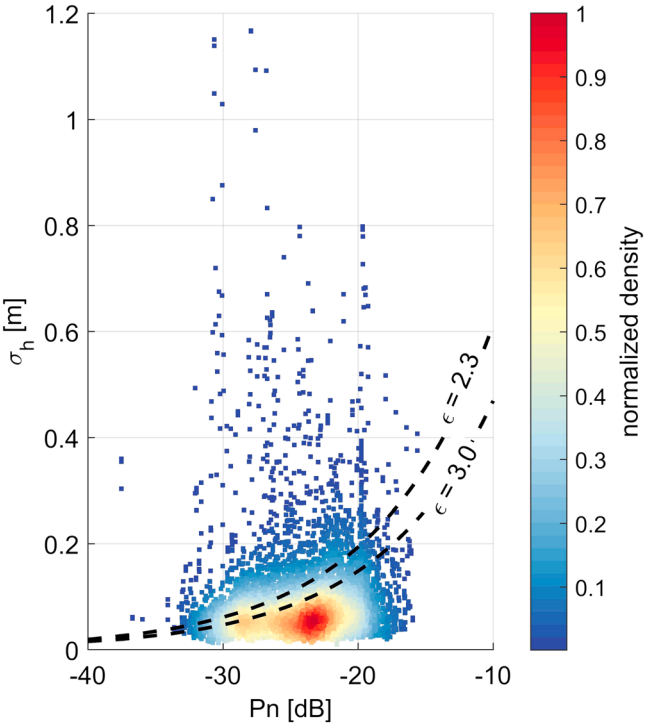

Figure 3. Normalized density plot of RSR-derived scattering components (P_n) against laser RMS surface roughness (σ_h) within the three firn zones. The black dotted lines represent the modeled theoretical scattering component for the given σ_h and permittivity values of 2.3 and 3.0. If the surface roughness was the major source of signal scattering, P_n values would lie along/between these lines.

spring 2004 to seek possible correlations between small-scale roughness features and P_n. The formation and orientation of sastrugi and the associated surface roughness are dependent on the prevailing wind pattern over the glacier surface [e.g., *Mather*, 1962]. Because similar patterns of katabatic winds and sastrugi formation have been observed over multiple years on DIC [*Koerner*, 1966; *Boon et al*., 2010], we argue that despite the 10 year time span between data collection, a comparison with roughness data from 2004 is meaningful. The small-scale surface roughness (10 cm point separation, 10 m baseline) ranges between 0.04 and 0.13 m and displays a general trend of increasing roughness with decreasing elevation (Figure 2b). However, no significant changes occur at the elevations where considerable shifts in P_n are observed (~1400 m and ~1800 m). This suggests that patterns in P_n are also not correlated to small-scale surface roughness. Thus, changes in the scattering signal component at the HiCARS instrument frequency are mainly caused by changes in the near-surface firn stratigraphy, while surface roughness effects are probably minor.

We assume that the winter snow pack has minimal effect on P_n. *Koerner* [1966] showed that the snow depth distribution over DIC does not vary systematically with elevation, so it is unlikely to covary with the observed distribution of P_n. Furthermore, the end-of-winter snow pack that existed during the measurement period was mostly homogeneous and dominated by a layered (deterministic) structure (a layer of wind-packed snow overlying depth hoar), which would contribute primarily to the reflectance component (P_c).

While theoretical backscattering models for a rough surface layer are well established [e.g. *Ulaby et al*., 1986; *Grima et al*., 2012], the formulation of models that capture effects of rough/undulating layers within the subsurface is more difficult [e.g., *Tabatabaeenejad and Moghaddam*, 2010; *Tabatabaeenejad et al*., 2013; *Zamani et al*., 2016]. Although a quantitative understanding of the scattering contribution from undulating ice layers in the firn facies of Zone II might explain the high P_n values in this zone, modeling such an effect is beyond the scope of this paper.

4. Conclusions

We calculated the scattering signal component of airborne RES surface echoes from DIC using the RSR method and compared the resulting pattern to the near-surface firn stratigraphy, which contains numerous ice layers formed by melting and refreezing processes. Three distinct facies zones occupy different elevation ranges and the scattered signal component changes significantly between them. Low scattering correlates with laterally homogeneous firn above 1800 m that contains thin, flat, and continuous ice layers and below 1200 m where firn predominantly consists of ice. Between 1200 and 1800 m, increased scattering coincides with firn containing inhomogeneous, undulating ice layers. Although backscattering theory suggests a correlation between surface roughness and scattered signal components, no such correlation was found

on DIC. Scattering values modeled for the observed surface roughness are significantly lower than the RSR-derived scattering values and failed to reproduce their spatial distribution pattern. Therefore, we conclude that changes in the scattering signal component on DIC are mainly generated by changes in the near-surface firn stratigraphy, although some contribution from surface roughness effects cannot be ruled out. Knowledge of the firn stratigraphy, especially the spatial extent of percolation features, is critical if repeat altimetry measurements of surface height derived from airborne or satellite sensors are used to estimate mass balance changes on Arctic ice caps. Our results suggest that the combined use of the RSR method and the scattering component from airborne-RES measurements has potential to characterize near-surface firn. This can help to identify areas where firn is affected significantly by melting and refreezing processes, areas for which mass balance estimates based on altimetrically-derived records of surface elevation change may have large uncertainties. This promising approach can easily be applied to other glaciers and ice caps which experience similar spatially and temporally inhomogeneous melting and refreezing processes. Finally, the RSR technique is being applied to planetary surfaces such as Mars [e.g., *Grima et al*., 2012] or two forthcoming missions to the icy moons of Jupiter [*Grima et al*., 2014a]; however, near-surface scattering effects are usually not considered. Our study will benefit planetary exploration by providing an improved understanding of the RSR-derived signal components and its relationship to near-surface properties.

Acknowledgments

This work was supported by grants from UK NERC (NE/K004999), NASA (13-ICEE13-00018), NSERC (Discovery Grant/Northern Research Supplement), Alberta Innovates Technology Futures, the CRYSYS Program (Environment Canada), and a University of Alberta Northern Research Award. We thank PCSP for logistical support, and NRI, NWB, and the peoples of Grise Fjord and Resolute Bay for research permission on Devon Ice Cap. A. Criscitiello, F. Habbal, G. Ng, C. Mortimer, S. Palmer, T. Richter, and many others helped with data collection. We also thank the Editor Julienne Stroeve and two anonymous reviewers for their helpful comments that improved the manuscript. This is UTIG contribution #3020. The data products derived for this study are available by contacting the corresponding author.

References

Bezeau, P., M. Sharp, D. Burgess, and G. Gascon (2013), Firn profile changes in response to extreme 21st-century melting at Devon Ice Cap, Nunavut, Canada, *J. Glaciol.*, *59*(217), 981–991, doi:10.3189/2013JoG12J208.

Boon, S., D. O. Burgess, R. M. Koerner, and M. J. Sharp (2010), Forty-seven years of research on the Devon Island Ice Cap, Arctic Canada, *Arctic*, *63*(1), 13–29.

Braithwaite, R. J., M. Laternser, and W. T. Pfeffer (1994), Variations of near-surface firn density in the lower accumulation area of the Greenland ice sheet, Pakitsoq, West Greenland, *J. Glaciol.*, *40*(136), 477–485, doi:10.1088/0022-3727/48/32/325305.

Cassidy, N. J. (2009), Ground penetrating radar data processing, modelling and analysis, in *Ground Penetrating Radar Theory and Applications*, edited by H. M. Jol, pp. 141–176, Elsevier, Amsterdam.

Cuffey, K. M., and W. S. B. Paterson (2010), *The Physics of Glaciers*, Academic Press, Oxford, U. K.

Destrempes, F., and G. Cloutier (2010), A critical review and uniformized representation of statistical distributions modeling the ultrasound echo envelope, *Ultrasound Med. Biol.*, *36*(7), 1037–1051, doi:10.1016/j.ultrasmedbio.2010.04.001.

Elfouhaily, T. M., and C.-A. Guérin (2004), A critical survey of approximate scattering wave theories from random rough surfaces, *Waves Random Media*, *14*(4), R1–R40, doi:10.1088/0959-7174/14/4/R01.

Fisher, D., J. Zheng, D. Burgess, C. Zdanowicz, C. Kinnard, M. Sharp, and J. Bourgeois (2011), Recent melt rates of Canadian arctic ice caps are the highest in four millennia, *Global Planet. Change*, *84–85*, 3–7, doi:10.1016/j.gloplacha.2011.06.005.

Gascon, G., M. Sharp, D. Burgess, P. Bezeau, and A. B. G. Bush (2013), Changes in accumulation-area firn stratigraphy and meltwater flow during a period of climate warming: Devon Ice Cap, Nunavut, Canada, *J. Geophys. Res. Earth Surf.*, *118*, 2380–2391, doi:10.1002/2013JF002838.

Gray, L., D. Burgess, L. Copland, M. N. Demuth, T. Dunse, K. Langley, and T. V. Schuler (2015), CryoSat-2 delivers monthly and inter-annual surface elevation change for Arctic ice caps, *Cryosphere*, *9*(5), 1895–1913, doi:10.5194/tc-9-1895-2015.

Grima, C., W. Kofman, A. Herique, R. Orosei, and R. Seu (2012), Quantitative analysis of Mars surface radar reflectivity at 20MHz, *Icarus*, *220*(1), 84–99, doi:10.1016/j.icarus.2012.04.017.

Grima, C., D. M. Schroeder, D. D. Blankenship, and D. A. Young (2014a), Planetary landing-zone reconnaissance using ice-penetrating radar data: Concept validation in Antarctica, *Planet. Space Sci.*, *103*, 191–204, doi:10.1016/j.pss.2014.07.018.

Grima, C., D. D. Blankenship, D. A. Young, and D. M. Schroeder (2014b), Surface slope control on firn density at Thwaites Glacier, West Antarctica: Results from airborne radar sounding, *Geophys. Res. Lett.*, *41*, 6787–6794, doi:10.1002/2014GL061635.

Harig, C., and F. J. Simons (2016), Ice mass loss in Greenland, the Gulf of Alaska, and the Canadian Archipelago: Seasonal cycles and decadal trends, *Geophys. Res. Lett.*, *43*, 3150–3159, doi:10.1002/2016GL067759.

Koerner, R. M. (1966), Accumulation on the Devon Island Ice Cap, Northwest Territories, Canada, *J. Glaciol.*, *6*(45), 383–392.

Kovacs, A., A. J. Gow, and R. M. Morey (1995), The in-situ dielectric constant of polar firn revisited, *Cold Reg. Sci. Technol.*, *23*(3), 245–256, doi:10.1016/0165-232X(94)00016-Q.

Mather, K. B. (1962), Further observations on sastrugi, snow dunes and the pattern of surface winds in Antarctica, *Polar Rec. (Gr. Brit.)*, *11*(4), 158–171, doi:10.1017/S0032247400052888.

Mortimer, C. A., M. Sharp, and B. Wouters (2016), Glacier surface temperatures in the Canadian High Arctic, 2000–15, *J. Glaciol.*, *62*(235), 963–975, doi:10.1017/jog.2016.80.

Parry, V., P. Nienow, D. Mair, J. Scott, B. Hubbard, K. Steffen, and D. Wingham (2007), Investigations of meltwater refreezing and density variations in the snowpack and firn within the percolation zone of the Greenland ice sheet, *Ann. Glaciol.*, *46*(1), 61–68, doi:10.3189/172756407782871332.

Peters, M. E., D. D. Blankenship, and D. L. Morse (2005), Analysis techniques for coherent airborne radar sounding: Application to West Antarctic ice streams, *J. Geophys. Res.*, *110*, B06303, doi:10.1029/2004JB003222.

Radić, V., and R. Hock (2011), Regionally differentiated contribution of mountain glaciers and ice caps to future sea-level rise, *Nat. Geosci.*, *4*(2), 91–94, doi:10.1038/ngeo1052.

Radić, V., A. Bliss, A. C. Beedlow, R. Hock, E. Miles, and J. G. Cogley (2013), Regional and global projections of twenty-first century glacier mass changes in response to climate scenarios from global climate models, *Clim. Dyn.*, *42*(5841), 37–58, doi:10.1007/s00382-013-1719-7.

Schroeder, D. M., C. Grima, and D. D. Blankenship (2016), Evidence for variable grounding-zone and shear-margin basal conditions across Thwaites Glacier, West Antarctica, *Geophysics*, *81*, WA35–WA43, doi:10.1190/geo2015-0122.1.

Sharp, M., D. O. Burgess, J. G. Cogley, M. Ecclestone, C. Labine, and G. J. Wolken (2011), Extreme melt on Canada's Arctic ice caps in the 21st century, *Geophys. Res. Lett.*, *38*, L11501, doi:10.1029/2011GL047381.

Tabatabaeenejad, A., and M. Moghaddam (2010), Study of validity region of small perturbation method for two-layer rough surfaces, *IEEE Geosci. Remote Sens. Lett.*, *7*(2), 319–323, doi:10.1109/LGRS.2009.2034543.

Tabatabaeenejad, A., X. Duan, and M. Moghaddam (2013), Coherent scattering of electromagnetic waves from two-layer rough surfaces within the kirchhoff regime, *IEEE Trans. Geosci. Remote Sens.*, *51*(7), 3943–3953, doi:10.1109/TGRS.2012.2229391.

Ulaby, F. T., R. K. Moore, and A. K. Fung (1986), *Microwave Remote Sensing, Active and Passive; Volume III, From Theory to Applications Remote Sensing, A Series of Advanced Level Textbooks and Reference Works*, Artech House, Dedham, Mass.

Vaughan, D. G., J. C. Comiso, I. Allison, J. Carrasco, G. Kaser, R. Kwok, and T. Murray (2013), IPCC observations: Cryoshpere, in *Climate Change 2013: The Physical Science Basis. Contribution of Working Group I to the Fifth Assessment Report of the Intergovernmental Panel on Climate Change*, pp. 317–382, Cambridge Univ. Press, Cambridge, U. K., and New York, doi:10.1017/CBO9781107415324.

Young, D. a., S. D. Kempf, D. D. Blankenship, J. W. Holt, and D. L. Morse (2008), New airborne laser altimetry over the Thwaites Glacier catchment, West Antarctica, *Geochem. Geophys. Geosyst.*, *9*, Q06006, doi:10.1029/2007GC001935.

Zamani, H., A. Tavakoli, and M. Dehmollaian (2016), Scattering from layered rough surfaces: Analytical and numerical investigations, *IEEE Trans. Geosci. Remote Sens.*, *54*(6), 3685–3692, doi:10.1109/TGRS.2016.2524639.